Filtering contaminants from a γ-sum spectrum: Measurement of the ^{94}Mo$(p, \gamma)^{95}$Tc cross section

R. Kelmar, J. P. McDonaugh, A. Simon,* J. O'Reilly, A. C. Dombos, A. Gula, J. Koros, M. Matney, O. Olivas-Gomez, D. Robertson, and E. Stech

Department of Physics and Astronomy, University of Notre Dame, Notre Dame, Indiana 46556-5670, USA

(Received 28 September 2022; revised 23 January 2024; accepted 13 February 2024; published 20 March 2024)

A measurement of the ^{94}Mo$(p, \gamma)^{95}$Tc cross section was performed. The cross section was measured in the energy range $E_{\text{c.m.}} = 1.5$–4.5 MeV, spanning essentially the entirety of the Gamow window relevant to the astrophysical γ process. The γ-summing technique was used to analyze the data. At lower energies the sum peak overlapped with peaks from the reaction ^{19}F$(p, \alpha\gamma)^{16}$O, so a new analysis method was developed to filter out the contamination from the this reaction. The measured cross section values were compared to the NON-SMOKER database. The measured cross sections show enhanced resonancelike features at low energies, which are not predicted in the NON-SMOKER code. The effects of this new measurement on the reaction rate were examined. It was found that there is a significant enhancement at lower temperatures in the (p, γ) reaction rate due to the enhancements found in the cross section.

DOI: 10.1103/PhysRevC.109.035805

I. INTRODUCTION

The so-called p nuclei are stable proton-rich isotopes of elements between selenium and mercury that are shielded by the valley of stability and thus cannot be accessed through β decay of neutron-rich isotopes. For that reason these nuclei cannot be produced via s and r processes. The astrophysical scenario that could reproduce the observed solar abundances of the p nuclei is the γ process proposed by Woosley *et al.* [1]. The γ process consists of a series of photodisintegration reactions on seed s-process nuclei and can occur, for example, in O-Ne layer of type II supernovae. It involves (γ, p), (γ, α), and (γ, n) reactions and requires temperatures in the range of 1.5–3.5 GK to reproduce the abundances of the solar p nuclei. An alternative scenario proposed by Frohlich *et al.* [2], the νp process, is a possible contributor to the abundances of the lighter p nuclei.

Several astrophysical scenarios have been proposed as possible sites for the γ process: a range of type II SN with various masses [3–5] and type Ia SN [6]. In the most recent work, galactic chemical evolution was also included in the modeling of the γ process [5,6]. All of the models are able to reproduce the observed abundances of the p nuclei within a factor of 2–3, however, the Mo and Ru p nuclei are known to be consistently underproduced by the models. ^{94}Mo has been consistently underproduced by all the models compated to the solar abundances. Though it is primarily produced via a series of (γ, n) reactions originating at ^{98}Mo, a fraction of the ^{94}Mo abundace originates from disintegration of ^{95}Tc via the ^{95}Tc$(\gamma, p)^{94}$Mo reaction [6]. Thus, in this work a measurement of the inverse reaction, ^{94}Mo$(p, \gamma)^{95}$Tc, is reported to help constrain the reaction rate for the disintegration reaction.

The experimental details are presented in Sec. II. The cross-section values obtained in this work are given and compared to literature values in Sec. III. The effect of the measurement on the reaction rate is investigated in Sec. IV. Finally, the conclusions are discussed in Sec. V.

II. EXPERIMENTAL METHOD

The experiment was conducted using the 5U accelerator [7]. A beam of protons with center-of-mass energies between 1.5 and 4.5 MeV was impinged upon a target of isotopically enriched ^{94}Mo. The beam current ranged from 5–900 nA and was increased at lower beam energies to compensate for the decreasing reaction cross section. The lower beam current was chosen at higher beam energies to maximize the count rate while maintaining the detector dead time below 1%. At lower energies the beam current was chosen to maximize count rate without impacting the target stability.

The ^{94}Mo target, 588(66) μg/cm^2 thick with 98.99% enrichment, was made by evaporation onto a gold backing. The gold backing, 96 mg/cm^2, was used to stop the beam at the target location to reduce the background contaminants from beam straggling, in particular fluorine that may be present in the beam-pipe components. The thickness of the target was verified using x-ray fluorescence. Detailed description of the targets and their preparation can be found in Ref. [8].

The targets were placed in the center of the high efficiency total absorption spectrometer (HECTOR). HECTOR [9] is composed of 16 NaI(Tl) segments each read by two photomultiplier tubes. These segments are arranged to cover nearly the entirety of the 4π solid angle. A collimator was placed 12 mm directly in front of the target location for tuning the beam

*anna.simon@nd.edu

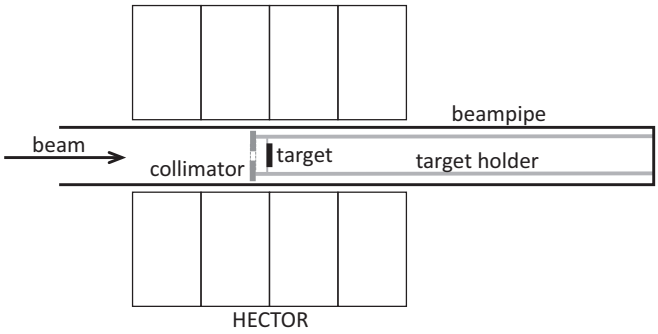

FIG. 1. Schematic of the target and collimator layout within the HECTOR borehole. The beam pipe is electrically isolated from the detector and from the beam line upstream to form a Faraday cup. The collimator, target, and target holder form one conductive element to collect the charge.

after energy changes. The collimator opening was 10 mm in diameter, which made it the same size as the target. During the runs the collimator was grounded to the beam pipe in order to accurately measure the beam current. The beam pipe was electrically isolated from the detector and from the beam line upstream of the detector and was utilized as a Faraday cup for measurements of the beam current. Figure 1 shows a sketch of the HECTOR setup with the locations of the target and the collimator within the setup. A lead brick wall was constructed on the upstream side of HECTOR to minimize the γ rays from beam interactions along the beam pipe.

The cross section was measured using the γ-summing technique [10]. When the ^{95}Tc that was produced in the reaction deexcites to the ground state, a cascade of γ rays is emitted. In the γ-summing technique all of the γ rays emitted in the cascade are summed up to give the total amount of energy detected during that event. The spectrum then consists of a single peak known as the sum peak. The energy of the sum peak is given by:

$$E_\Sigma = E_{\text{c.m.}} + Q, \tag{1}$$

where $E_{\text{c.m.}}$ is the center-of-mass energy of the system and Q is the Q value of the reaction. In this case the Q value is 4.896 MeV.

With the γ-summing technique the cross section is given by:

$$\sigma = \frac{N_\Sigma}{N_b n_t \varepsilon_\Sigma}, \tag{2}$$

where N_Σ is the dead time corrected number of counts in the sum peak, N_b is the total number of beam particles, n_t is the areal target density, and ε_Σ is the summing efficiency.

An example of an experimental sum peak corresponding to a center-of-mass energy of 4 MeV is shown in Fig. 2. The sum peak is clearly seen just below 9 MeV. The peak is fit with a Gaussian and a first-order polynomial. The first-order polynomial is then used to subtract off the background under the peak that comes from incomplete summations. The peak can then be integrated to determine the N_Σ needed to calculate the cross section. The efficiency of HECTOR is then determined from GEANT4 simulations of γ-ray cascades with the same

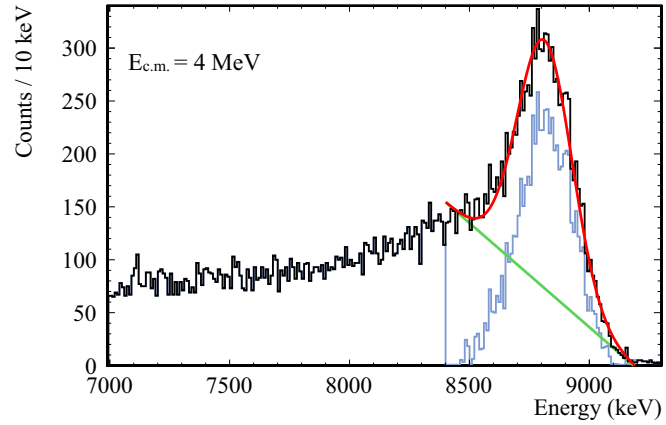

FIG. 2. An example of the fitting procedure used to fit the sum peaks. A combination of a Gaussian on a linear background is used. The light blue shows the linear-background-subtracted histogram that is integrated to obtain the number of counts in the sum peak.

total energy and with an average γ-ray multiplicity matched to that of the reaction of interest. This is the standard method used to analyze HECTOR data and is described in detail in Ref. [9].

A. Spectra contamination from ^{19}F$(p, \alpha\gamma)^{16}$O reaction

The measurements discussed here posed an additional challenge. For beam energies below 2.6 MeV, the sum peak of interest started to overlap with contaminant lines present in the sum spectrum that stem from the ^{19}F$(p, \alpha\gamma)\,^{16}$O reaction. The ^{16}O populated by this reaction deexcited via emission of three well-known γ rays at energies of 6.1, 6.9, and 7.1 MeV. Additionally, the ^{19}F$(p, \alpha\gamma)\,^{16}$O reaction cross section is much higher than that of the reaction of interest, thus even minute amounts of ^{19}F result in strong lines in the spectrum in the 6–7 MeV range. With the decreasing cross section for the ^{94}Mo$(p, \gamma)^{95}$Tc reaction, the sum peak of interest was comparable with the lines from ^{16}O (Fig. 3). With that, the standard

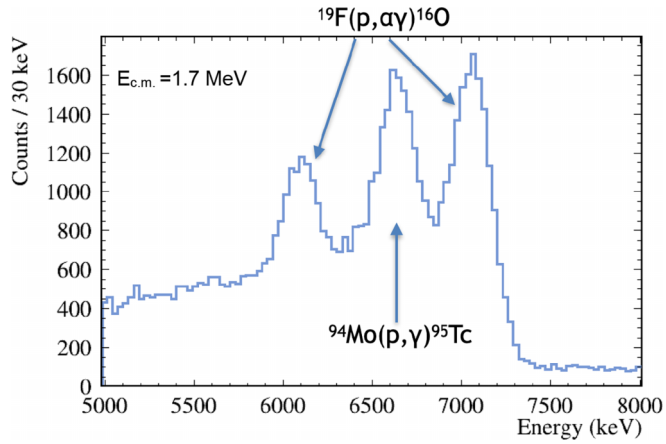

FIG. 3. An example of a sum peak that is overlapping with the peaks from the reaction ^{19}F$(p, \alpha\gamma)\,^{16}$O. The sum peak of interest cannot be disentangled from the contamination peaks in this case.

analysis procedure for HECTOR could not be applied directly to the experimental data at energies below 2.6 MeV.

In order to eliminate the contaminants from the spectrum, a filter was developed to remove the peaks from the ^{19}F$(p,\alpha\gamma)\,^{16}$O reaction during the off-line analysis. The basic principles of the filter take into account the fact that the states in ^{16}O all decay directly to the ground state via a single γ ray, while the reaction of interest generally decays via multiple γ rays. This fact, along with the segmentation of HECTOR, allowed for the separation of the true events from the reactions of interest and those originating from the contamination.

For each event detected by HECTOR the number of segments that fired, i.e., recorded a γ ray, is determined. The segment multiplicity (here referred to as multiplicity) M, is proportional to the γ-ray multiplicity N_γ which is the number of γ rays in the deexcitation cascade. This quantity is the crucial signature that allows for separation of the true events from the contaminants.

Since the decay of ^{16}O consists of a single γ-ray, most of the energy from that γ ray will be deposited in a single crystal or two neighboring crystals if the γ ray Compton scatters. Thus, the expected event multiplicity in HECTOR will be $M = 1$ or 2. On the other hand, the ^{95}Tc decays via a cascade of several γ rays, which are emitted isotropically. In such case, the energy will be dispersed more evenly throughout the crystals and typically a higher number of crystals, $M = 4$–5, will fire. With the above in mind, the filter was designed to eliminate the ^{16}O contaminants. The filter employs the following steps:

(1) Any event where more than 4 MeV is deposited in a single crystal is ignored. The cutoff of 4 MeV was determined for this data set to maximize the fraction of contaminants to be removed while at the same time minimizing the fraction of true events that were eliminated.
(2) For any event involving only two or three crystals, if the event included two neighboring crystals it is ignored.

The filter was tested with data recorded with a blank gold backing in which some ^{19}F was present. The backing was irradiated with a proton beam within the energy range identical to that used for the reaction of interest. Data was taken in 50 keV steps across the whole energy range to investigate the evolution of the contaminant spectra with beam energy and to test the filter for various branchings of the ^{16}O lines. The results of this filtering process can be seen in Fig. 4. Figure 4(a) shows a spectrum with just the peaks from the ^{19}F$(p,\alpha\gamma)\,^{16}$O, the blue spectrum shows two distinct peaks, while the black spectrum, which has been passed through the filter, is now just a flat background. Figure 4(b) shows the results when a ^{94}Mo data run is passed through the filter. The contamination peaks are completely eliminated and there is still a clear sum peak from the reaction of interest. This remaining peak can the be analyzed using the same fitting procedure as before. It is clear from the figure that some of the events of interest are also removed by the filter. This is accounted for in the procedure for determining HECTOR's summing efficiency.

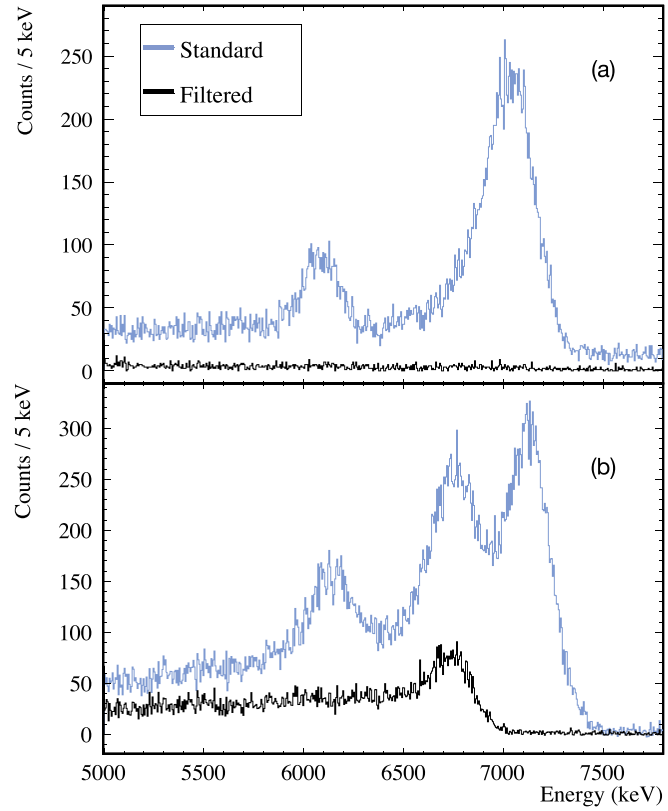

FIG. 4. Examples of the sum spectrum after using the filtering process. (a) shows spectra for a gold backing where only the ^{19}F$(p,\alpha\gamma)\,^{16}$O peaks are present. In the standard spectrum, blue line, the peaks are clearly visible, while in the filtered spectrum, black line, there is just a flat background present. (b) shows the effect on a data taken for the ^{94}Mo target. In the standard, blue, spectrum there are three peaks, but in the filtered, black, spectrum there is just one peak left, the real sum peak of interest.

B. Summing efficiency

The summing efficiency in Eq. (2) is determined through GEANT4 simulations. For this purpose, random cascades of γ rays that sum up to the sum peak energy are generated and passed through a GEANT4 simulation of HECTOR. The cascades are generated with a wide range of γ multiplicities to account for various possible deexcitation paths. While in the experimental data the average number of γ rays in the cascades cannot be determined, it is correlated with the average number of segments $\langle M\rangle$ that fired during the events. The same quantity can be extracted from the simulation. Then, the summing efficiency is determined from the simulated events that match the value of $\langle M\rangle$. This method has been described in detail in Refs. [9,11] and applied to several measurements using HECTOR [12,13].

For the analysis employed in this work, the filter that was applied to the data is very sensitive to the details of the γ cascades that are passed through it. Thus, in order to correctly determine HECTOR's efficiency for filtered data, the

generated γ cascades must very closely model the deexcitation of ^{95}Tc populated by the ^{94}Mo$(p,\gamma)^{95}$Tc reaction. One approach to this is to use codes such as DICEBOX [14] or RAINIER [15] to generate the γ cascades using statistical properties of the nuclei of interest. However, this would required fine tuning of the parameters of the level density and the γ-ray strength function models as the cascades generated using the default parameters that are implemented in those codes do not reproduce the details of the experimental spectra. Instead, for this work cascades were generated using a Monte Carlo code with a set of conditions based on the known details of the ^{95}Tc level scheme fine tuned to reproduce the experimental spectra. The cascades were generated as a sequence of random γ rays originating from the high-density states at higher energies followed by deexcitation via known discrete γ rays. The main points that needed to be taken into account are as follows:

(i) The cascades must include γ rays corresponding to the deexcitations between the low-lying discrete levels of ^{95}Tc. The intensities of those lines must match those observed in the experiment.
(ii) The energy of the continuum γ rays must be restricted by providing a low-energy limit. This eliminates cascades that include unrealistic γ ray energies.
(iii) The γ-ray multiplicities of the cascades must be fine tuned, so that the values of $\langle M \rangle$ from the simulation match those of the experimental data.

To develop this new process, runs where the sum peak was between 7 and 8 MeV were analyzed using both the standard method and the filter method. The selected runs were as close to the energy range where the filter was needed as possible, while ensuring that no contamination is present within the sum peak. For those runs, both analysis methods should yield the same cross-section value. In total, there were six runs that matched these criteria.

In order to fine tune the details of the cascades, spectra from individual segments of HECTOR obtained during the experiment were compared with the results of the simulations. A sum-of-segments spectrum was created by requiring only events with the total energy deposited to be within $\pm 3\sigma$ of the sum-peak centroid. For higher statistics, the spectra from all 16 segments were added together. Each simulations included 10^6 cascades that were used to generate the simulated spectra. 10^3 simulations were performed to generate a heat map—a distribution of the simulation results that could be compared to the experimental data.

1. Discrete γ rays in the cascades

The first step was to look at the sum-of-segments histogram, to identify any individual γ rays that are particularly strong. This can be seen in Fig. 5. Figure 5(a) shows the sum peak, in black, and the region that was gated on to generate the sum-of-segments spectrum. It also shows the variation in the simulated histograms, plotted as a heat map. Figure 5(b) shows the sum-of-segments histogram, in black, corresponding to the sum peak energy, with the heat map showing the final simulation results.

The decay branching that was found to be the most important for the accuracy of the efficiency simulations was the direct decay to the ground state. This is due to the fact that the filter is designed to get rid of single γ-ray events, thus it will eliminate all direct-decay events from the data set. To determine this branching, the events in the sum peak region with multiplicity of one [Fig. 5(c)] were analyzed. All of the high-energy runs where the sum peak did not overlap with the contamination peaks were used in order to determine a linear relationship for how the amount of direct decays changed with energy. Figure 5(c) shows the excellent agreement that was achieved. This relationship was then used to extrapolate the branching ratio needed at the lower energies.

The two strongest γ rays observed [Fig. 5(b)] were the transitions to the ground state from the second and third excited states in ^{95}Tc at 336 and 626 keV, respectively. Also visible are γ rays corresponding to the states at 748 and 1236 keV. The generated cascades were adjusted so that the experimentally observed intensities of those lines were reproduced by the simulations. Using the sum-of-segments spectra for each of the specific multiplicities the γ-ray branching that matched the experimental data could be determined. Figure 5(d) shows the sum-of-segments for multiplicity two events. This same spectrum was made for all multiplicities up to 5 to ascertain that there was good agreement.

2. Constraints on the continuum γ rays

The second parameter that impacted the simulated spectra was the energy range of the γ rays from the continuum. Those γ rays are generated using a uniform distribution and their energies are limited so that the total energy is equal to that of the sum peak. In order to reproduce the fine details of the sum-of-segment spectra, a lower limit had to be set for the energies of γ rays generated in the cascades. However, a hard cutoff limit would result in an artificial peak in the spectrum, thus a blurring parameter was introduced to correct for that. The blurring parameter provides a range from which the lower energy limit can be drawn. As a result, the lower energy limit varied from cascade to cascade allowing for blurring of the cutoff value.

These two parameters were varied systematically to achieve the closest agreement in the calculated cross sections obtained from analysis with and without the filter on the six test runs selected. As a result both the lower limit of the γ-ray energies and the blurring factor were set to 550 keV.

3. γ-ray multiplicities

The last parameter that was investigated was the maximum number of γ rays per cascade. If this value is too high, the simulated efficiency will be artificially reduced. If it is too low, the variety of the decay cascades will not be represented correctly in the simulation and the efficiency may be overestimated. This parameter can be adjusted based on the segment multiplicity plots. Figure 6 shows the comparison between experimental data and the simulations. Figure 6(a) shows the comparison between the standard multiplicity distributions, while Fig. 6(b) shows the comparison between the filtered distributions. In both cases the experimental data is well

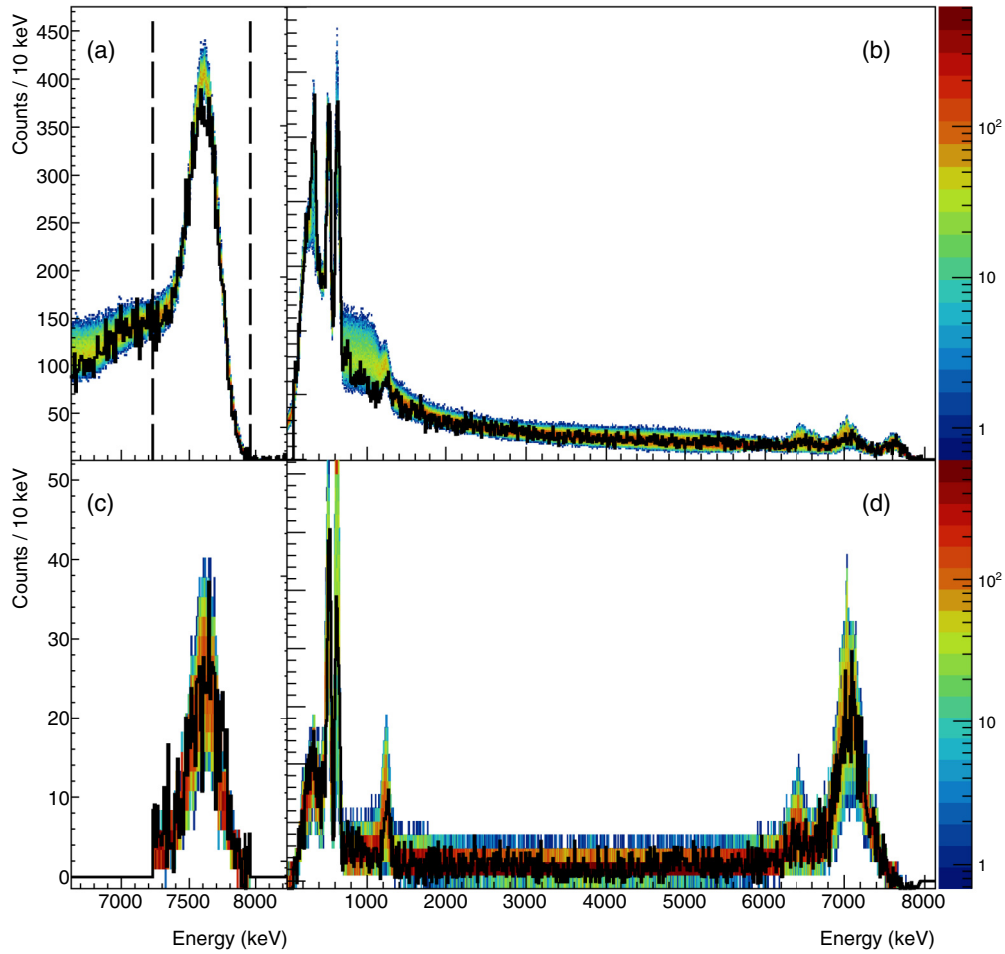

FIG. 5. An example of the comparison between an experimental run (black) and all of the matching simulations (heat map) for the final set of input parameters. (a) shows the sum peak, the dashed lines indicate a gate on the sum peak used to generate (b)–(d). (b) shows the individual segment energies that correspond to the events within the gated region. (c) shows the events corresponding to the sum peak with a multiplicity of 1, and (d) shows the same for events with a multiplicity of 2.

reproduced by the simulations as follows the center of the heat map.

4. Comparison of the two efficiency simulations

The two methods to determine HECTOR's efficiency—the original one from Ref. [9] and the one developed for this work—were applied to the ^{94}Mo$(p,\gamma)^{95}$Tc reaction data. For beam energies above 2.6 MeV the filter was not necessary. Here the sum peak was analyzed as in Ref. [9], while the efficiency was calculated from both methods. In both cases, as can be seen in Fig. 7, resulting cross sections are in a very good agreement with each other.

For energies below 2.6 MeV, the sum peak overlapped with the contaminant lines in the sum spectrum, thus the filter was used to eliminate the contaminants. Again, the efficiency was determined using the two methods. The simulated data was passed through the filter to account for the events eliminated from the experimental data. It is clear from Fig. 7 that the new method yields a smooth continuation between the high- and low-energy data points. The original efficiency simulations do not capture the details of the cascades correctly, leading to incorrect modeling of the efficiency and an underestimated cross section visible here as an offset in the red data set.

C. Uncertainty quantification

Each of the components of the cross-section formula has an uncertainty, which is accounted for in the uncertainty of the cross section. The number of beam particles has a systematic uncertainty of 5%. The uncertainty in the number of events in the sum peak consists of the statistical uncertainty from the number of events. This was less than 10% for all of the runs. The dead time was less than 1% and had minimal impact on the uncertainty. The relative uncertainty of the summing efficiency was around 5% for the standard analysis runs and around 20% for the runs analyzed using the filter. The uncertainty in the target thickness was 11%.

The uncertainty in the center-of-mass energy comes from a combination of the uncertainty in the beam energy resolution and the energy loss through the target. The beam resolution from the 5U has an uncertainty of 1–2 keV and the energy loss through the targets ranged between 20 and 60 keV.

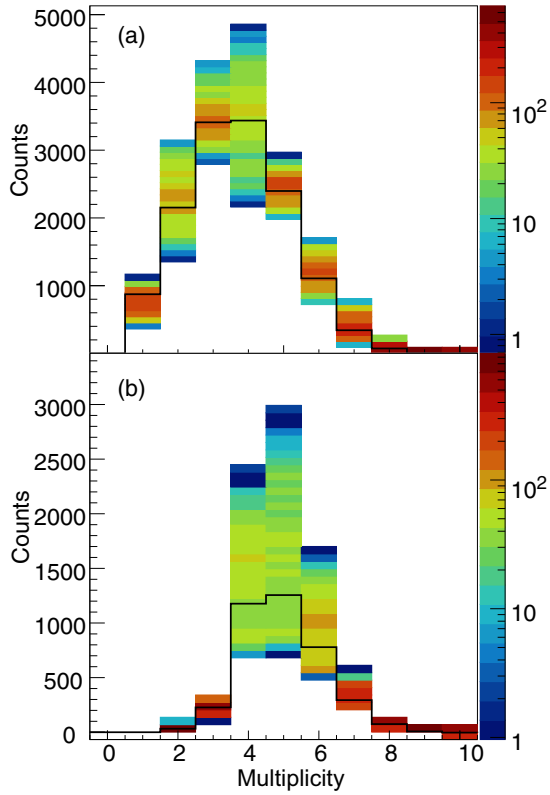

FIG. 6. An example of the comparison of the M between the same experimental run (black) as Fig. 5 and all of the matching simulations (heat map) for the final set of input parameters. (a) shows the comparison of the standard M, while (b) shows the comparison of the M of the events that make it through the filter. It both cases there is good agreement between the experimental run and the distribution from the simulations.

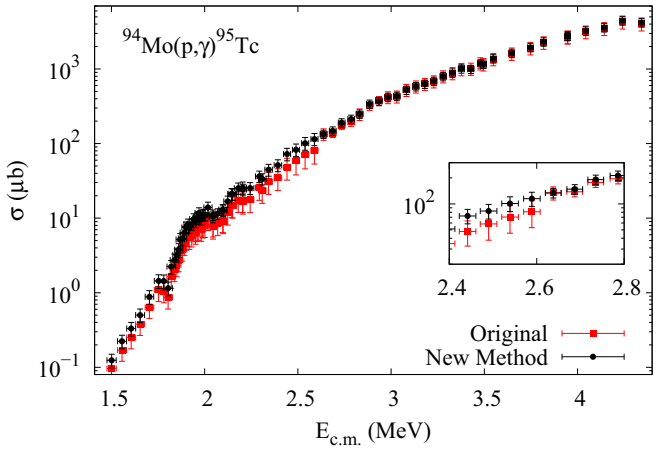

FIG. 7. The cross sections for the ^{94}Mo(p, γ)^{95}Tc reaction using the original efficiency method developed in Ref. [9] compared to the results with the extended method. For the higher-energy runs where the filter is not used there is excellent agreement between the two methods, and these extra steps are not necessary. For the runs where the filter is used there is a systematic offset between the two methods.

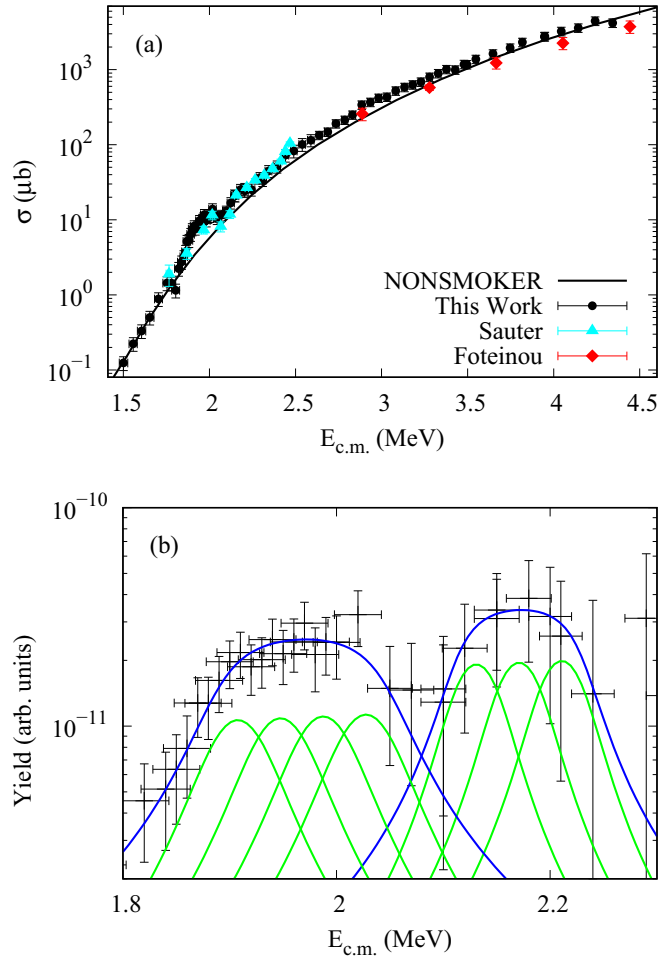

FIG. 8. Panel (a) shows measured cross sections (black squares) for the ^{94}Mo(p, γ)^{95}Tc reaction. Excellent agreement is seen with the previous measurements by Sauter *et al.* (blue triangles [16]) and Foteinou *et al.* (red diamonds [17]). The cross sections are also compared to theoretical Hauser Feshbach calculations done using the NON-SMOKER code [18]. Panel (b) shows a possible analysis of the structures around 2 MeV. The yield with the underlying background curve subtracted has been fit as a series of narrow resonances. The blue curves show the total fit to the structures while the green curves show the theoretical contribution from narrow underlying resonances.

III. RESULTS

The cross sections for the ^{94}Mo(p, γ)^{95}Tc reaction are shown in Fig. 8(a) and the data points are listed in Table I. The cross section was measured between $E_{c.m.}$ = 1.5–4.5 MeV. Two previous measurements exist within this energy range. At the lower energies, excellent agreement with the results of Sauter *et al.* [16] can be observed as the results of this work overlap within the error bars with those from Ref. [16]. At higher energies, the results of this work are in a good agreement with those from Ref. [17] with at most 20% deviation from our data at the highest energies. This work connects the two previous measurements and provides a more detailed scan of the cross section. With this what looks like a random scatter

TABLE I. Measured cross-section values for ^{94}Mo$(p,\gamma)^{95}$Tc.

$E_{c.m.}$[MeV]	σ[μb]
1.501(25)	0.124(0.026)
1.557(24)	0.223(0.046)
1.606(24)	0.331(0.068)
1.654(24)	0.501(0.104)
1.704(23)	0.88 (0.18)
1.753(23)	1.44 (0.30)
1.781(23)	1.43 (0.30)
1.804(23)	1.15 (0.24)
1.821(23)	2.40 (0.50)
1.838(23)	2.75 (0.56)
1.851(22)	3.22 (0.65)
1.861(22)	3.76 (0.79)
1.869(22)	5.2 (1.0)
1.881(22)	5.3 (1.1)
1.891(22)	6.4 (1.3)
1.9 (22)	7.5 (1.4)
1.911(22)	8.2 (1.5)
1.918(22)	7.6 (1.3)
1.931(22)	8.2 (1.4)
1.942(22)	9.7 (1.7)
1.951(22)	9.0 (1.6)
1.96 (22)	10.0 (1.8)
1.966(22)	10.5 (1.8)
1.97 (22)	11.7 (2.1)
1.982(22)	9.83 (1.8)
1.991(22)	10.9 (1.9)
2.001(22)	11.2 (2.0)
2.018(22)	13.9 (2.5)
2.045(21)	10.4 (1.7)
2.07 (21)	11.5 (1.9)
2.097(21)	13.0 (2.2)
2.099(21)	12.6 (2.0)
2.124(21)	16.8 (2.9)
2.145(21)	21.2 (3.7)
2.15 (21)	20.9 (3.7)
2.18 (21)	25.2 (4.4)
2.204(20)	25.7 (4.8)
2.205(20)	24.2 (4.3)
2.244(20)	25.3 (4.6)
2.293(20)	36.3 (6.4)
2.309(20)	33.6 (5.8)
2.343(20)	44.6 (8.1)
2.393(20)	51.3 (9.4)
2.442(19)	73(14)
2.49 (19)	83(16)
2.539(19)	101 (20)
2.589(19)	115 (21)
2.638(18)	134 (17)
2.687(18)	148 (19)
2.735(18)	191 (24)
2.786(18)	213 (27)
2.831(18)	250 (32)
2.885(17)	340 (44)
2.935(17)	369 (48)
2.983(17)	419 (54)
3.031(17)	432 (56)
3.082(17)	523 (68)
3.133(16)	584 (76)
3.181(16)	630 (82)
3.229(16)	687 (89)
3.279(16)	797 (103)
3.329(16)	889 (115)
3.377(16)	1010 (130)
3.428(16)	995 (127)
3.479(15)	1180 (152)
3.496(15)	1170 (151)
3.548(15)	1380 (178)
3.647(15)	1630 (211)
3.747(15)	1950 (253)
3.818(15)	2320 (301)
3.946(14)	2750 (357)
3.948(14)	2780 (364)
4.044(14)	3240 (426)
4.143(14)	3600 (469)
4.241(14)	4450 (584)
4.343(14)	4190 (547)

in the Sauter data is shown to be resonancelike structures in the cross section around 2 MeV.

Figure 8(a) also compares the results to cross sections predicted using the NON-SMOKER model [18]. The NON-SMOKER model uses the Hauser-Feshbach (HF) formalism to calculate cross sections. The HF formalism assumes that in the excited state energy range populated in the reaction there is a high enough level density that the properties of the excited states can be treated statistically instead of as individual levels. In this case the NON-SMOKER model does a good job reproducing the overall shape and strength of the cross sections, except for the structures observed around 2 MeV. The HF assumption of statistical properties leads to the prediction of a smoothly varying cross section.

Since the structures around 2 MeV are not predicted by the HF formalism, all known sources of contamination were examined to determine that these structures are indeed a feature of the ^{94}Mo$(p,\gamma)^{95}$Tc cross section. As mentioned earlier, the Sauter *et al.* [16] measurements also showed scatter in this energy range and since that measurement was done using the activation technique, it is therefore not sensitive to the same contamination from the ^{19}F$(p,\alpha\gamma)^{16}$O reaction. This rules out the ^{19}F$(p,\alpha\gamma)^{16}$O reaction as a possible source of contamination. Additionally, since the structures appear in the energy range where the filter was used any other reactions that result in a single γ ray would also be filtered out. Another possible source of contamination in a summing detector would be if there was a resonance at these energies for a nucleus with a similar Q value as the reaction of interest. All of the nuclei with a similar Q value and all of the ones that could possibly have a resonance anywhere near these energies have distinct γ rays in their decays that would be seen in the sum-of-segments

spectra. In order to be able to explain the strength of the observed structures that contaminant reaction would have to be at least as strong as the actual reaction of interest, and since the only γ rays observed are those associated with the decay of ^{95}Tc these resonances in contaminant materials can be ruled out.

In the literature, Bork *et al.* [19] reported similar scatter in the ^{96}Ru$(p,\gamma)^{97}$Rh cross section. This reaction has a similar Q value and is also two neutrons away from the neutron magic number. This makes it a good comparison. It has also been observed that in the Tc isotopes as they get closer to the neutron magic number, which occurs at ^{93}Tc, there is a strong decrease in the level density, with ^{95}Tc having a density of states that is five times less than that of ^{97}Tc [20]. This lower level density could mean that the assumption of statistical levels is not appropriate at the lower energy range, leading to the discrepancy with the NON-SMOKER predictions.

The structures reported here are around 160 keV wide and the energy loss through the targets was only ≈40 keV in this energy range, so the structures are too wide to be individual resonances. If it is assumed that the structures are made up of multiple resonances that are too close in energy to be resolved given the target thickness, then four evenly spaced resonances with a resonance strength ≈8 eV or three evenly spaced resonances with a resonance strength of ≈11 eV would explain the strength of the full features. This is shown in Fig. 8(b). The total fits to the background subtracted yields are shown in blue while the contribution from the theoretical individual resonances are shown in green.

IV. REACTION RATES

To examine the impact of this measurement on the astrophysical modeling the reaction rate needs to be calculated. The reaction can be calculated from the cross section by:

$$N_A\langle\sigma v\rangle = \left(\frac{8}{\pi\mu}\right)^{1/2}\frac{1}{(kT)^{3/2}}\int_0^\infty E\sigma(E)e^{-E/kT}dE, \quad (3)$$

where N_A is Avogadro's constant, μ is the reduced mass, kT is the thermal energy, E is the center-of-mass energy, and $\sigma(E)$ is the corresponding total cross section.

Since the cross section was mapped out in detail over nearly the entire energy range corresponding to the Gamow window for the γ process, the cross section was numerically integrated rather than relying on a fit to the data. Even though the integral in Eq. (3) over the cross section is from 0 to infinity, only the energy range within the Gamow window is necessary to obtain the reaction rate since the Maxwell-Boltzmann distribution quickly drops off at higher temperatures and the Coulomb penetrability quickly drops off at lower temperatures. This allowed for investigation of the effects of the resonancelike structures on the reaction rate, which are not predicted by the HF models normally used.

The reaction rate obtained with this work can be seen in Fig. 9 in blue. The green line is the rate given in the REACLIB database [21]. These rates are assumed to have an uncertainty of a factor of 3 [22]. This uncertainty is depicted by the green shaded region. The uncertainty band obtained for this work is shown in blue. The uncertainty of the reaction rate

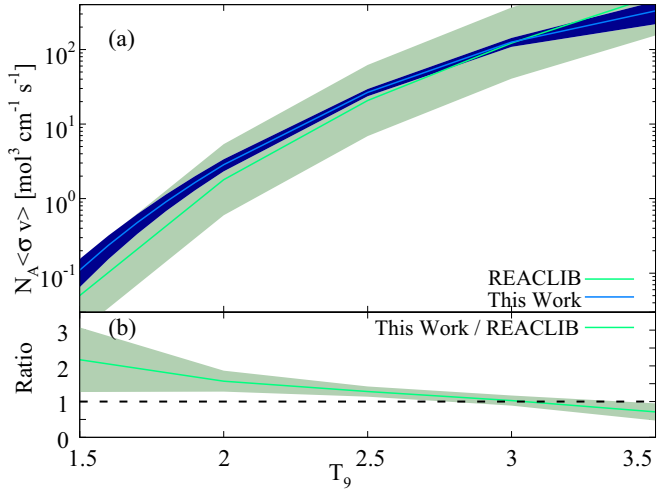

FIG. 9. The astrophysical reaction rate for the ^{94}Mo$(p,\gamma)^{95}$Tc reaction. The green line is the rate given in the REACLIB [21] database. The green band is a factor of 3 uncertainty. The blue line is the result of this work and the shaded region represents the 3σ uncertainty. The bottom panel shows the ratio between this work and the REACLIB rate. It is close to 1 above 2 GK. Below 2 GK it diverges and is about a factor of 2 stronger.

was obtained by performing a Monte Carlo technique. The cross-section values were randomly sampled from a Gaussian distribution with the mean and standard deviation from the measured point and then the integral was computed. This process was repeated 100 000 times to obtain a probability distribution for the true value of the reaction rate at each temperature. The blue band represents the 3σ uncertainty range for the reaction rate. At temperatures below 2 GK, the rates obtained here are about a factor of 2 higher than the REACLIB rates.

Across the whole temperature range of the γprocess the REACLIB rates agree with the measured rates within the uncertainty. However, this work is able to greatly reduce the uncertainty in the reaction rate. Additionally, the measured rate shows a strong enhancement at the low temperatures when compared to the REACLIB rate. This comes from the resonancelike structures that are not present in the NON-SMOKER cross section. The rates calculated in this work are given in Table II.

V. CONCLUSIONS

This work measured the reaction ^{94}Mo$(p,\gamma)^{95}$Tc from $E_{\text{c.m.}} = 1.5$–4.5 MeV. The cross section was carefully mapped out in step sizes ranging from 10–50 keV. In order to measure the lower-energy points a new filtering method had to be developed to separate out the real signal from the reaction and the contamination from the reaction ^{19}F$(p,\alpha\gamma)^{16}$O. Then the method for calculating the summing efficiency had to be adapted to account for the use of the filter on the data. With these new methods, excellent agreement with the past measurements [16,17] is seen.

Additionally, this work provides a much more detailed scan of the ^{94}Mo$(p,\gamma)^{95}$Tc reaction across the entire Gamow

TABLE II. The recommended reaction rates for the ^{94}Mo$(p,\gamma)^{95}$Tc and the ^{95}Tc$(\gamma,p)^{94}$Mo reactions.

T [GK]	$N_A\langle\sigma v\rangle$ [cm^{3}mol^{-1}s^{-1}]	λ [s^{-1}]
1.5	0.109(15)	$6.9(2.9)\times10^{-09}$
1.6	0.237(28)	$3.5(1.2)\times10^{-07}$
1.7	0.477(47)	$5.3(1.6)\times10^{-06}$
1.8	0.908(76)	$9.9(2.4)\times10^{-05}$
1.9	1.643(12)	$8.4(1.7)\times10^{-04}$
2	2.85(17)	$6.0(1.1)\times10^{-03}$
2.5	26.60(99)	$2.28(.25)\times10^{+01}$
3	125.7(5.7)	$6.01(.84)\times10^{+03}$
3.5	330(37)	$1.84(.53)\times10^{+05}$

window for the γ process. The detailed mapping allowed for the confirmation of resonancelike structures around 2 MeV. The reaction rate was then calculated by numerically integrating the measured cross sections. The resonancelike structures were found to increase the reaction rate at low temperatures.

ACKNOWLEDGMENTS

This research utilized resources from the University of Notre Dame Center for Research Computing and was supported by the National Science Foundation under the Grants No. PHY-1614442, No. PHY-2011890 (NSL), and No. PHY-1430152 (JINA-CEE).

[1] S. E. Woosley and W. M. Howard, Astrophys. J., Suppl. Ser. **36**, 285 (1978).
[2] C. Fröhlich, G. Martínez-Pinedo, M. Liebendörfer, F.-K. Thielemann, E. Bravo, W. R. Hix, K. Langanke, and N. T. Zinner, Phys. Rev. Lett. **96**, 142502 (2006).
[3] W. Rapp, J. Görres, M. Wiescher, H. Schatz, and F. Käppeler, Astrophys. J. **653**, 474 (2006).
[4] M. Pignatari, K. Göbel, R. Reifarth, and C. Travaglio, Int. J. Mod. Phys. E **25**, 1630003 (2016).
[5] C. Travaglio, T. Rauscher, A. Heger, M. Pignatari, and C. West, Astrophys. J. **854**, 18 (2018).
[6] C. Travaglio, R. Gallino, T. Rauscher, F. K. Röpke, and W. Hillebrandt, Astrophys. J. **799**, 54 (2015).
[7] Notre Dame Nuclear Science Laboratory, www.isnap.nd.edu (September 2022).
[8] R. Kelmar, K. Manukyan, A. Simon, and A. Aprahamian, Nucl. Instrum. Methods Phys. Res., Sect. A **1034**, 166763 (2022).
[9] C. S. Reingold, O. Olivas-Gomez, A. Simon, J. Arroyo, M. Chamberlain, J. Wurzer, A. Spyrou, F. Naqvi, A. C. Dombos, A. Palmisano, T. Anderson, A. M. Clark, B. Frentz, M. R. Hall, S. L. Henderson, S. Moylan, D. Robertson, M. Skulski, E. Stech, S. Y. Strauss *et al.*, Eur. Phys. J. A **55**, 77 (2019).
[10] A. Spyrou, H.-W. Becker, A. Lagoyannis, S. Harissopulos, and C. Rolfs, Phys. Rev. C **76**, 015802 (2007).
[11] O. Olivas-Gomez, A. Simon, D. Robertson, A. C. Dombos, F. Strieder, T. Kadlecek, M. Hanhardt, R. Kelmar, M. Couder, J. Görres, E. Stech, and M. Wiescher, Eur. Phys. J. A **58**, 57 (2022).
[12] O. Olivas-Gomez, A. Simon, O. Gorton, J. E. Escher, E. Churchman, P. Millican, R. Kelmar, C. S. Reingold, A. M. Clark, N. Cooper, C. Harris, S. L. Henderson, S. E. Kelly, F. Naqvi, A. Palmisano, D. Robertson, E. Stech, A. Spyrou, and W. P. Tan, Phys. Rev. C **102**, 055806 (2020).
[13] A. C. Dombos, D. Robertson, A. Simon, T. Kadlecek, M. Hanhardt, J. Görres, M. Couder, R. Kelmar, O. Olivas-Gomez, E. Stech, F. Strieder, and M. Wiescher, Phys. Rev. Lett. **128**, 162701 (2022).
[14] F. Bečvář, Nucl. Instrum. Meth. Phys. Res. A **417**, 434 (1998).
[15] L. Kirsch and L. Bernstein, Nucl. Instrum. Meth. Phys. Res. A **892**, 30 (2018).
[16] T. Sauter and F. Käppeler, Phys. Rev. C **55**, 3127 (1997).
[17] V. Foteinou, M. Axiotis, S. Harissopulos, P. Dimitriou, G. Provatas, A. Lagoyannis, H.-W. Becker, D. Rogalla, A. Zilges, A. Schreckling, and A. Endres, Eur. Phys. J. A **55**, 67 (2019).
[18] T. Rauscher and F.-K. Thielemann, At. Data Nucl. Data Tables **79**, 47 (2001).
[19] J. Bork, H. Schatz, F. Käppeler, and T. Rauscher, Phys. Rev. C **58**, 524 (1998).
[20] D. A. Close and R. C. Bearse, Nucl. Phys. A **201**, 337 (1973).
[21] R. H. Cyburt, A. M. Amthor, R. Ferguson, Z. Meisel, K. Smith, S. Warren, A. Heger, R. D. Hoffman, T. Rauscher, A. Sakharuk, H. Schatz, F. K. Thielemann, and M. Wiescher, Astrophys. J., Suppl. Ser. **189**, 240 (2010).
[22] T. Rauscher, Phys. Rev. C **73**, 015804 (2006).